ENVIRONMENTAL RESEARCH
LETTERS

LETTER • OPEN ACCESS

How has the North Pacific Gyre Oscillation affected peak season tropical cyclone genesis over the western North Pacific from 1965 to 2020?

To cite this article: Yifei Dai *et al* 2022 *Environ. Res. Lett.* **17** 104016

ENVIRONMENTAL RESEARCH
LETTERS

OPEN ACCESS

RECEIVED
14 July 2022

REVISED
11 August 2022

ACCEPTED FOR PUBLICATION
15 August 2022

PUBLISHED
21 September 2022

LETTER

How has the North Pacific Gyre Oscillation affected peak season tropical cyclone genesis over the western North Pacific from 1965 to 2020?

Yifei Dai[1], **Bin Wang**[2,3], **Na Wei**[1,4,*], **Jinjie Song**[1,4] **and Yihong Duan**[4]

[1] Nanjing Joint Institute for Atmospheric Sciences, Nanjing 210041, People's Republic of China
[2] Department of Atmospheric Sciences and International Pacific Research Center, University of Hawaii at Manoa, Honolulu, HI 96822, United States of America
[3] Earth System Modeling Center, Nanjing University of Information Science and Technology, Nanjing 210044, People's Republic of China
[4] State Key Laboratory of Severe Weather, Chinese Academy of Meteorological Sciences, Beijing 100081, People's Republic of China
[*] Author to whom any correspondence should be addressed.

E-mail: weina@cma.gov.cn

Keywords: tropical cyclone, North Pacific Gyre Oscillation, Western North Pacific, decadal variations

Abstract

The North Pacific Gyre Oscillation (NPGO) is an important mode of decadal variability in North Pacific sea surface temperature (SST) and sea surface height. This study investigated the potential influence of the NPGO on spatial characteristics of peak season (July to October) tropical cyclone genesis (TCG) number over the western North Pacific (WNP) from 1965 to 2020. We show that the NPGO was the first leading empirical orthogonal function mode of North Pacific SST during the peak tropical cyclone season in that time. On a decadal time scale, the NPGO has opposite impacts on TCG in the west and east WNP. The relatively weak positive correlation west of 140° E and the strong negative correlation east of 140° E result in an overall significant negative correlation between the NPGO and WNP total TCG number ($r = -0.49$), which is much more robust than the relationship between the Pacific Decadal Oscillation and TCG. The critical factors of the NPGO that affect TCG are vertical motion in the west WNP and vertical wind shear (VWS) in the east WNP. The positive NPGO pattern could induce an anomalous off-equatorial vertical circulation, resulting in an upward motion and increased convective precipitation in the west WNP, favoring local TCG. The anomalous convective precipitation enhances the zonal gradient of the atmospheric heat source in the east WNP, increasing VWS. The North Pacific low-level anticyclonic and upper-level cyclonic associated with the NPGO further enhance the VWS in the east WNP and lead to the negative low-level relative vorticity, inhibiting local TCG. This study emphasizes the importance of the climate impact of the NPGO in recent decades. The findings here have significant implications for the decadal prediction of change in WNP TCG.

1. Introduction

The western North Pacific (WNP), including the South China Sea, is the most active basin of tropical cyclone (TC) activity. About one-third of global TCs, with an annual average of 33 TCs, are formed in this basin (Emanuel 2018). TCs are usually accompanied by heavy rainfall and strong wind, threatening the daily lives of billions of people and causing an enormous economic loss each year (Zhang *et al* 2009, Li *et al* 2022). On the other hand, TCs bring abundant moisture from tropical oceans to East Asian countries, benefiting local agriculture to a certain extent (Ren *et al* 2006). It is essential to better predict WNP TC activity and mitigate damage. Hence, further efforts should be made to understand the key processes and underlying mechanisms causing the long-term change in WNP TC activity.

In the last few decades, WNP TC activity has experienced pronounced decadal change, with distinct active and inactive periods (Hong *et al* 2016). A significant decadal reduction in TC genesis (TCG)

number over the WNP was observed after the 1990s, and both the location and tracks of TCG have moved northward (Hong *et al* 2016, Cao *et al* 2020, Zhao *et al* 2022). Extensive research has been conducted to investigate the causes of this long-term change in WNP TC activity, but the exact mechanisms are yet to be determined (Li and Zhou 2018). Several natural variabilities in sea surface temperature (SST) are reported to be associated with the recent changes in the WNP TC activity, including the Pacific Decadal Oscillation (PDO; Hong *et al* 2016), the North Pacific Gyre Oscillation (NPGO, or Victoria mode; Zhang *et al* 2013, Pu *et al* 2019), El Niño–Southern Oscillation (ENSO; Wang and Chan 2002), the Atlantic Multidecadal Oscillation (Wang *et al* 2022) and Indian Ocean SST (Wang *et al* 2013).

Among these natural variabilities, ENSO and PDO are the most concerning interannual and decadal drivers of WNP TC activity. The Eastern Pacific ENSO (EP-ENSO) and PDO are the first leading modes of interannual variation in tropical Pacific SST and decadal variation in North Pacific SST, respectively (Mantua *et al* 1997, Wang *et al* 2019). Various studies have pointed out that ENSO and PDO have pronounced impacts on both the number and location of TCG by regulating large-scale atmospheric circulation and ocean thermal conditions, leading to a southeastward movement of TCG during the positive PDO phase or El Niño year (e.g. Wang and Chan 2002, Wang *et al* 2010, Zhao and Wang 2019).

However, during the past few decades, variances of second-leading modes of Pacific SST on both interannual and decadal time scales have significantly increased. On an interannual time scale, Central Pacific (CP)-El Niño events have occurred more frequently than EP-El Niño events since the 1990s (Wang *et al* 2019). Numerous studies have pointed out that CP-ENSO is better related to the WNP TCG number than EP-ENSO (e.g. Liu and Chen 2018, Patricola *et al* 2018, Song *et al* 2021). Some studies have also attributed the decadal reduction of TCG number after 1998 to more CP-ENSO occurrences (Zhao and Wang 2019). On a decadal time scale, the contribution of the NPGO to Pacific SST variability has increased, and variance of the NPGO has been comparable to that of the PDO during the past few decades (Litzow *et al* 2020). However, compared with CP-ENSO, there are few studies on the relationship between the NPGO and WNP TC activity (Zhang *et al* 2013, Pu *et al* 2019).

As the second leading mode of Pacific SST and sea surface height (SSH), the NPGO could efficiently modulate the large-scale circulations associated with TC activity (Di Lorenzo *et al* 2008). For example, some studies have pointed out that a positive NPGO pattern could strengthen the ascending branch of Walker circulation over the WNP and enhance moisture transportation from tropical oceans to the mid-low latitude WNP (Ye *et al* 2016, Hu *et al* 2018). Moreover, research has indicated that the PDO is closely related to EP-ENSO, while the NPGO is better associated with CP-ENSO (Di Lorenzo *et al* 2010), suggesting a possible pathway by which the NPGO may affect TC activity via CP-ENSO. Given the increase in CP-ENSO events and the increased impact of the NPGO on variances in Pacific SST, the NPGO may play a more important role in the change in WNP TCs in recent decades than most imagine. Pu *et al* (2019) pointed out that the spring NPGO (or Victoria mode) could be used to predict the May to August change in WNP TCG. Zhang *et al* (2013) found that the total TCG number over the WNP is better related to the NPGO than PDO. However, the spatial distribution of the simultaneous relationship between the NPGO and WNP TCG during the peak TC season (from July to October, JASO) and the underlying mechanisms have rarely been studied.

The present work addresses how the NPGO has affected the spatial distribution of WNP TC activity on a decadal time scale over the recent half-century. The remainder of this paper is organized as follows. Section 2 describes the data and methodology used in this study. Section 3 exhibits the relationship between WNP TC activity and the NPGO and explores the plausible physical mechanisms. In section 3, two specific questions are addressed: (a) What are the spatial characteristics of WNP TCG associated with the NPGO? (b) What key processes or large-scale environmental control the impact of the NPGO on WNP TCG? Section 4 presents the summary and discussions.

2. Data and method

2.1. Data

The TC best-track dataset over the WNP was obtained from the International Best Track Archive for Climate Stewardship version 4 (IBTrACS v4; Knapp *et al* 2018) for the years 1965–2020. The IBTrACS contains 6 h records (four times a day) of TC position and maximum sustained surface wind reported by several agencies. To minimize the uncertainty among data sources, we adopted TC records from two agencies, the Joint Typhoon Warning Center and the Japan Meteorological Agency. We only use the TC records with the 1 min sustained surface wind speed greater than 34 knots. The TCG position is where the maximum sustained surface wind first reaches 34 knots. WNP TCs occur every month, but the most active TC season is in JASO. This study primarily focuses on TCG in JASO over the WNP. To analyze the spatial–temporal variation, we transformed the raw data into both $2^\circ \times 2^\circ$ and $5^\circ \times 5^\circ$ grids by counting TCG at each grid point. Then, a nine-point weighted smoother is applied to improve spatial continuity while the weights are calculated based on the inverse distance interpolation algorithm of Lu and Wong (2008).

The monthly NPGO index processed by Di Lorenzo *et al* (2008) can be accessed at www.o3d.org/npgo/npgo.php (last accessed 13 May 2022). The monthly PDO index is obtained from the National Oceanic and Atmospheric Administration (NOAA) National Centers for Environmental Information, which is based on NOAA's Extended Reconstructed SST version 5 (ERSST v5) dataset and closely follows the Mantua PDO index (Mantua *et al* 1997). The monthly mean SST is derived from NOAA ERSST v5 (Huang *et al* 2017) with a horizontal resolution of 2° × 2° for the years 1965–2020. Monthly mean precipitation and atmospheric circulation data, including the zonal and meridional wind speed, vertical velocity and relative and specific humidity, were obtained from the fifth generation of the European Centre for Medium-range Weather Forecasts Reanalysis (Hersbach *et al* 2020) with a horizontal resolution of 0.25° × 0.25°. All SST and atmosphere circulation data were interpolated to a 2° × 2° grid. We removed the linear trend of all observational data.

2.2. Methodology

We used two empirical genesis indices to figure out the combined impacts of large-scale atmospheric and oceanic conditions on TCG. The first is the genesis potential index proposed by Emanuel and Nolan (2004), hereafter the ENGPI. Formulation of the ENGPI is as follows:

$$\mathrm{ENGPI} = \left|10^5\eta\right|^{\frac{3}{2}}\left(\frac{H}{50}\right)^3\left(\frac{\mathrm{MPI}}{70}\right)^3(1+0.1Vs)^{-2}$$

where η is the absolute vorticity at 850 hPa (s^{-1}), H is the relative humidity at 600 hPa (%), MPI is the maximum potential intensity (m s^{-1}) and Vs is the vertical wind shear (VWS) between 200 hPa and 850 hPa (m s^{-1})

$$\mathrm{MPI} = A + B\mathrm{e}^{C(T-T_0)}.$$

MPI is calculated according to the parameterization scheme proposed by Knaff *et al* (2005), in which MPI is only a function of SST, and the maximum allowed value of MPI is 185 knots. The coefficients are provided as $A = 38.21$ kt, $B = 170.72$ kt, $C = 0.1909\ ^\circ\mathrm{C}^{-1}$ and $T_0 = 30.0\ ^\circ\mathrm{C}$.

The second index is the dynamic genesis potential index (DGPI) proposed by Wang and Murakami (2020). Formulation of the DGPI is as follows:

$$\mathrm{DGPI} = (2+0.1\times Vs)^{-1}\left(5.5-\frac{\partial u}{\partial y}\times 10^5\right)^2 \times(5-20\times\omega)^3\left(5.5+\left|10^5\times\eta\right|\right)^2\mathrm{e}^{-11}-1$$

where η and Vs are the same as those in the ENGPI, $\frac{\partial u}{\partial y}$ is the meridional gradient of zonal wind at 500 hPa (s^{-1}) and ω is the vertical pressure velocity at 500 hPa (Pa s^{-1}).

Empirical orthogonal function (EOF) analysis decomposes the temporal–spatial variation into a series of temporal–spatial orthogonal modes according to the eigenvalues and eigenvectors of the covariance matrix computed from the original dataset (Lorenz 1956). Each leading EOF mode is described by a spatial pattern and a time-varying sequence (also known as the principal component, PC). The eigenvectors rank the EOF modes, and the first leading EOF mode accounts for the largest covariance of the original dataset. North's test examines the separability of each leading EOF mode (North *et al* 1982). The statistical significance of linear correlation and regression is determined by Student's t-test. Because the low-pass filter tends to decrease the degrees of freedom, the effective degrees of freedom, which consider autocorrelation sequences with a lagged window, are used in this study (Xiao and Li 2007).

3. Results

3.1. Temporal and spatial relationship between the NPGO and TCG

A conventional way to describe variation of the NPGO is to use the index provided by Di Lorenzo *et al* (2008). This NPGO index was reconstructed based on the second leading EOF mode of the monthly North Pacific SST or SSH during the last 50 years of the 20th century, which primarily reflects its change in the boreal winter season. However, Litzow *et al* (2020) mentioned that a North Pacific climate shift in the late 1980s resulted in large-scale change in climate patterns over multidecadal time scales. To concentrate on the impact of the NPGO on peak season TCG in recent decades, we apply the EOF method to normalized JASO mean SST over the North Pacific from 1965 to 2020.

Figures 1(a) and (b) show regressed peak season SST with reference to PCs of the first two leading EOF modes of the North Pacific SST (hereafter PC1 and PC2). Surprisingly, we find that the first leading EOF mode shows a NPGO-like pattern, accounting for ∼25% of the total variance, and the PDO-like pattern becomes the second EOF mode. PC1 is used to represent peak season NPGO variation in this study. The positive NPGO-like pattern is characterized by positive SST anomalies over the mid-west North Pacific and negative SST over the northeast North Pacific and tropical central Pacific (TCP). The PDO-like pattern is still the first leading EOF mode of winter SST and annual SST, accounting for nearly 30% of the total variance (figure not shown). Nevertheless, the NPGO becomes the first leading EOF mode of the North Pacific SST in the peak TC season. This again emphasizes the importance of the NPGO and its potential influence on climate in recent decades, especially during the boreal summer.

As shown in figure 1(c), WNP TCG exhibits pronounced interannual and decadal periods, while PC1

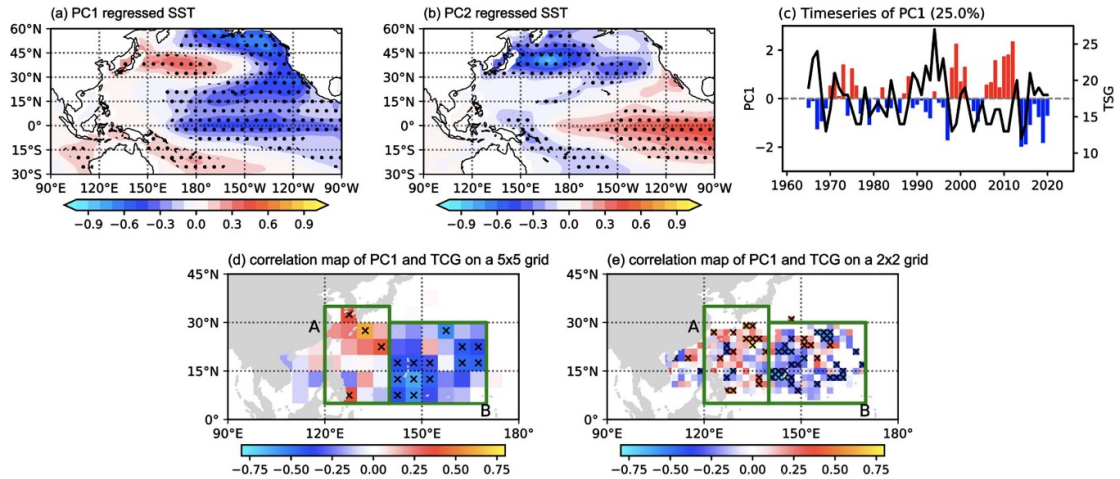

Figure 1. The regressed JASO mean SST with reference to original time series of PCs of the first two leading EOF modes of simultaneous North Pacific SST (a), (b) from 1965 to 2020, respectively (in °C). Bar charts in (c) show the time series of the PCs of the first leading EOF modes. The black curve in (c) indicates the interannual variation of WNP total TCG. (d), (e) Correlation maps between the decadal component of WNP TCG and PC1 from 1965 to 2020 on the 2° × 2° (d) and 5° × 5° grid (e). The green boxes in (d) and (e) outline the major regions of significant positive (region A, 5° N–35° N, 120° E–140° E) and negative (region B, 5° N–30°N, 140° E–170° E) correlation. Dots and × indicate that the correlation coefficients are statistically significant at a 95% confidence level. The effective degrees of freedom on a decadal time scale in (d) range from 28 to 35 among different grid points.

primarily exhibits significant decadal periods. A spectrum analysis further identifies that both TCG and PC1 have a 12 year peak (figure not shown). To focus on a decadal time scale, we then apply a 7 year low-pass Butterworth filter to TCG, PC1 and all other observational data. In this way, the interannual signals are largely removed, especially the variations associated with ENSO, and the quasi-decadal and decadal signals are retained (Zhang *et al* 2013, Wu *et al* 2020). The following analysis is conducted based on the decadal components.

The correlation coefficient between PC1 and WNP TCG is −0.49 ($P < 0.01$) on a decadal time scale, while that of PC2 and WNP TCG is only 0.11. The results here corroborate those of Zhang *et al* (2013), in which the NPGO is more robustly correlated with WNP total TCG than the PDO on a decadal time scale. In addition, we compared PC1 with the NPGO index (derived from the NPGO website; Di Lorenzo *et al* 2008). On a decadal time scale, the correlation coefficient between PC1 and the NPGO index is 0.83. Meanwhile, our results show that PC1 and PC2 can well describe the independent impacts of NPGO and PDO indices on WNP total TCG number. The partial correlation between NPGO index and WNP TCG with the effect of the PDO index removed is −0.43 ($P < 0.01$), while that between the PDO index and TCG with the impact of the NPGO index removed is −0.01, which is close to the linear correlation coefficients between PC1, PC2 and TCG.

We then studied the spatial characteristics of the relationship between the NPGO and TCG. Figure 1(d) shows the correlation map of PC1 and TCG. The TCG pattern associated with the NPGO (PC1) shows an east–west dipole pattern, and this dipole is robust on different horizontal grids. The negative correlations are statistically significant at the 95% confidence level in most regions of the east WNP (region B, 140° E–170° E). The positive correlations in the west WNP are relatively weaker. Positive correlations are observed in most areas of the west WNP but more than half of them are of minor insignificance at the 95% confidence level (figures 1(d) and (e)). Such an asymmetric dipole correlation pattern results in a significant negative correlation between the WNP total TCG number and PC1.

3.2. Large-scale conditions

What controls the NPGO–WNP TCG relationship on a decadal time scale? Favorable conditions for TCG include a lower VWS, higher SST and upper ocean heat content, lower atmospheric stability, abundant water vapor at the mid-low troposphere (relative humidity, RH) and positive relative vorticity (Emanuel 2005). We estimate the contribution of each environmental field to TCG change and identify the key factors based on two empirical genesis indices, ENGPI (Emanuel and Nolan 2004) and DGPI (Wang and Murakami 2020).

Figures 2(a) and (b) show the spatial distribution of PC1-regressed ENGPI and ENGPI anomalies. The ENGPI anomaly refers to the change of ENGPI when PC1 increases by 1.5 standard deviations. As shown in the figure, ENGPI could reproduce the west positive and east negative seesaw pattern of the PC1–TCG relationship, although the diagnosed positive PC1–ENGPI relationship is overestimated relative to the PC1–TCG relationship.

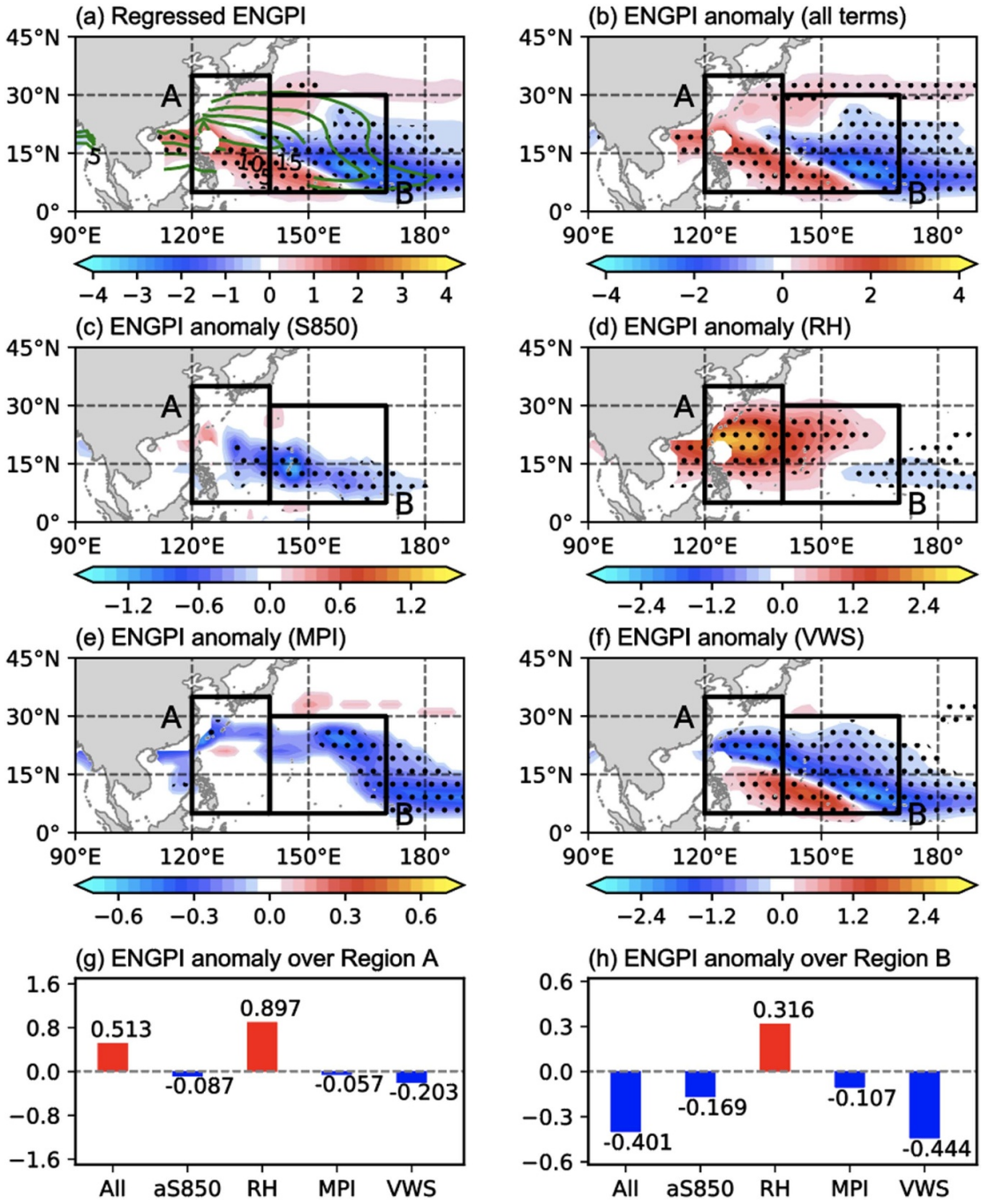

Figure 2. (a) The regression field of the ENGPI index with respect to PC1. JASO mean ENGPI anomaly associated with PC1-regressed changes in (b) total anomalies, (c) 850 hPa relative vorticity (S850), (d) 600 hPa relative humidity (RH), (e) maximum potential intensity (MPI) and (f) 850–200 hPa vertical wind shear (VWS), respectively. The mean contributions of each term to ENGPI anomalies over region A and region B are shown in panel (g). Dots indicate that the regression coefficient is statistically significant at the 95% confidence level. The black boxes outline the same region as that in figure 3. The green contours on panel (a) show ENGPI climatology from 1965 to 2020.

We further calculated the ENGPI anomaly, in which only one term is varied (PC1 increases by 1.5 standard deviations) and other terms are fixed at their long-term climatology (figures 5(c)–(f)). In this way, we could estimate each factor's contribution to TCG, including S850, RH, VWS and MPI (Wang *et al* 2022). In region A, a positive NPGO pattern could lead to favorable conditions of positive anomalies of RH (figure 2(c)), which corresponds fairly well to the positive NPGO–TCG relationship. However, NPGO also induces the negative anomaly of S850 in region A, which suppresses the TCG and weakens the positive NPGO–TCG relationship. The positive NPGO pattern enhances VWS in the north of region A, which is unfavorable to TCG. Meanwhile, weakened VWS is observed in the south of region A, which is conducive to TCG. Thus, the impact of NPGO-induced VWS on ENGPI in region A is primarily offset. In region B, the negative anomalies of S850 and MPI and positive anomalies of VWS are all harmful to

TCG, contributing to the negative NPGO–TCG relationship. However, the positive anomalies of RH are also observed at most grid points in region B, which favors TCG, thereby weakening the negative correlation between NPGO and TCG. The above evidence confirms that the NPGO could affect TC activities by regulating the large-scale conditions over the WNP, although it would induce both favorable and unfavorable conditions. It is a reasonable next step to quantify the contribution of different fields and identify the main factors.

Figures 2(g) and (h) summarize the mean ENGPI anomalies contributed by each term in the ENGPI formula over regions A and B, respectively. In region A, the increase in ENGPI (0.513 counts) is primarily caused by the positive anomalous RH (175%, 0.897 counts), while VWS exerts a relatively weak negative contribution of about −40% (−0.203 counts) to the ENGPI increase. The contributions of S850 and MPI to change in ENGPI are negligible. In region B, the contributions of different factors to changes in ENGPI are more complicated than in region A. The reduction of ENGPI (−0.401 counts) is mainly caused by the weakened VWS (111%, −0.444 counts), while the increasing RH makes a large contribution of about 79% (0.316 counts) to increasing ENGPI. Meanwhile, S850 also provides a non-negligible contribution of about 42% (−0.169 counts) to the decrease in ENGPI in region B.

As a comparison, we also analyze each term's contribution to TCG change based on the DGPI formula. DGPI includes no thermodynamic factors and only four dynamic factors, including S850, VWS, 500 hPa omega and 500 hPa meridional gradient of the zonal wind. Wang and Murakami (2020) pointed out that DGPI performs better in representing the interannual variation of TCG over the WNP. As shown in figures 3(a) and (b), the magnitude of anomalous DGPI in the east WNP is stronger than that in the west WNP. Such an asymmetric seesaw structure, i.e. strong negative east and relatively weak positive west, indicates the better skill of DGPI in reproducing the PC1–TCG relationship than ENGPI on a decadal time scale.

Spatial distributions and the regional mean of DGPI anomaly caused by changes in different factors are shown in figures 3(c)–(h). The DGPI anomaly caused by VWS and S850 is similar to that of the ENGPI. The meridional gradient of zonal wind shows a north–south contrast pattern, so its impact on DGPI is primarily offset. Mid-level omega is the most important factor for the increased DGPI over region A. In region B, the decrease in DGPI is a combined effect of multivariable change, in which the VWS and 850 hPa vorticity contribute about 91% and 49%, respectively. The meridional gradient of zonal wind and omega have relatively weak negative contributions of about −18% and −21%, respectively.

Overall, both DGPI and ENGPI indicate that the NPGO-induced anomalous VWS, in additon to low-level relative vorticity, are the main factors for TCG change in region B. In region A, DGPI suggests that 500 hPa omega is the primary factor from the dynamics aspect, while ENGPI suggests that 600 hPa RH is the key factor from the thermodynamics aspect. The next question is, for the PC1–TCG relationship, which indicator is better, mid-level RH or omega? Or are RH and omega of equal importance?

A cautious note is that in a region of ascending motion, the upward transport of moisture from the boundary layer would increase the mid-level relative humidity, resulting in a high correlation between 500 hPa vertical velocity and 600 hPa RH (Wang and Murakami 2020). In region A, the correlation coefficient between 600 hPa RH and 500 hPa omega is −0.88 on a decadal time scale. However, as mentioned above, the positive PC1–ENGPI relationship in region A is overestimated compared with that between PC1 and TCG, which is caused by anomalous RH. Also, RH makes a large negative contribution to ENGPI change in region B, suggesting that RH may be misinformed in the NPGO–TCG relationship. We would not deny that abundant moisture is conducive to TCG, but the results suggest that ENGPI may vastly overestimate the importance of RH on the NPGO–TCG relationship over the WNP. Ma and Fei (2022) pointed out that TCs can also be stably sustained via the supply of surface sensible heat instead of latent heat. As a comparison, the 500 hPa omega-induced DGPI change in region A is smaller than the RH-induced ENGPI change. 500 hPa omega shows a negligible effect in region B, which is more reasonable than RH. Hence, 500 hPa omega is a better indicator for the NPGO–TCG decadal relationship than 600 hPa RH over the WNP.

We next investigate how the NPGO produces the spatial patterns of anomalous VWS, mid-level omega and low-level relative vorticity. The dipole SST pattern of the NPGO in the extratropical North Pacific would lead to an anomalous meridional circulation that connects the extratropical and tropical Pacific, resulting in anomalous SST over the TCP (Di Lorenzo *et al* 2008, Ye *et al* 2016). In this case, a positive NPGO is associated with the negative SST anomaly in the tropical central and eastern Pacific (TCEP; south of 30° N, figure 4(a)). In low-latitude oceans, surface SST largely determines the surface wind convergence (Lindzen and Nigam 1987). Therefore, the negative SST anomaly in the TCEP would reduce precipitation in the North Pacific Intertropical Convergence Zone (figure 4(b)). According to the Matsuno–Gill theory, the reduced precipitation heating in the tropics would stimulate a descending Rossby wave response (Matsuno 1966, Gill 1980). The Rossby wave response of anomalous cooling is featured as a low-level anticyclonic

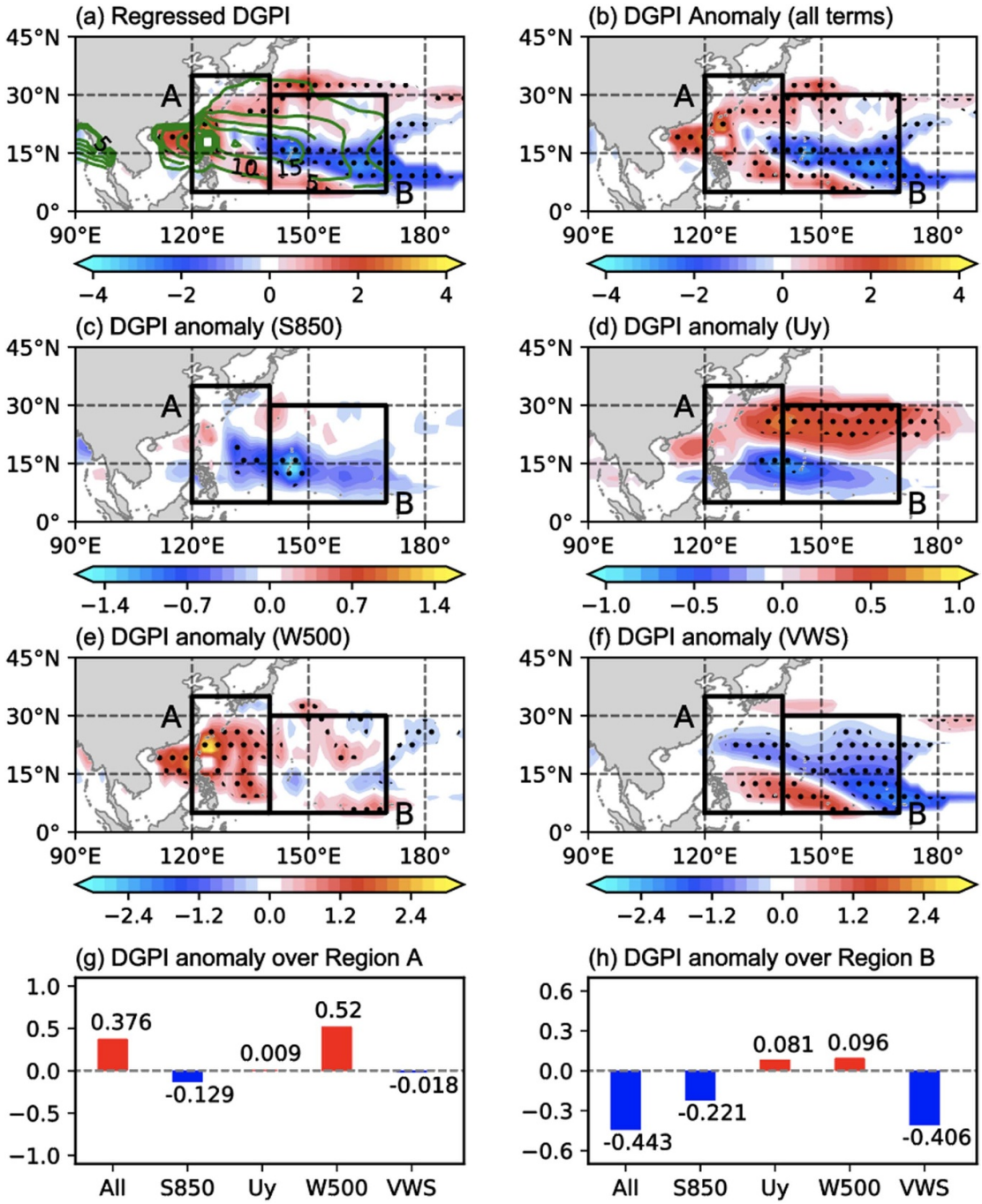

Figure 3. Same as figure 2 but for DGPI. (a) PC1-regressed field of DGPI. (b)–(f) JASO mean DGPI anomaly associated with PC1-regressed changes in (b) total anomalies, (c) 850 hPa relative vorticity (S850), (d) 500 hPa meridional gradient of zonal wind (Uy), (e) 500 hPa omega (W500) and (f) 850–200 hPa vertical wind shear (VWS), respectively. The mean contributions of each term to DGPI anomalies over regions A and B are shown in panels (g) and (h), respectively.

and upper-level cyclonic anomalous circulation system over the northwest of the cooling center in the Northern Hemisphere (figures 4(c) and (d); Hoskins and Wang 2006, Cai *et al* 2022). This anomalous circulation system resembles the North Pacific Oscillation (Rogers 1981).

The sinking motion and opposite low-level and high-level circulation establish an anomalous off-equatorial east–west secondary circulation (figure 4(h)), resulting in strong upward motion over the southwest of the low-level anticyclonic system (figure 4(e)). The ascent enhances local precipitation, releasing a large amount of latent heat in region A. The heating in region A and cooling in the central Pacific largely increase the large-scale zonal gradient of the atmospheric heat source in region B. Then, according to thermal wind theory, the increasing gradient of the heat source enhances the VWS in region B. On the other hand, out-of-phase low-level and high-level circulations are observed in region B, resulting in anomalous low-level easterlies and high-level westerlies in the southern region B and low-level

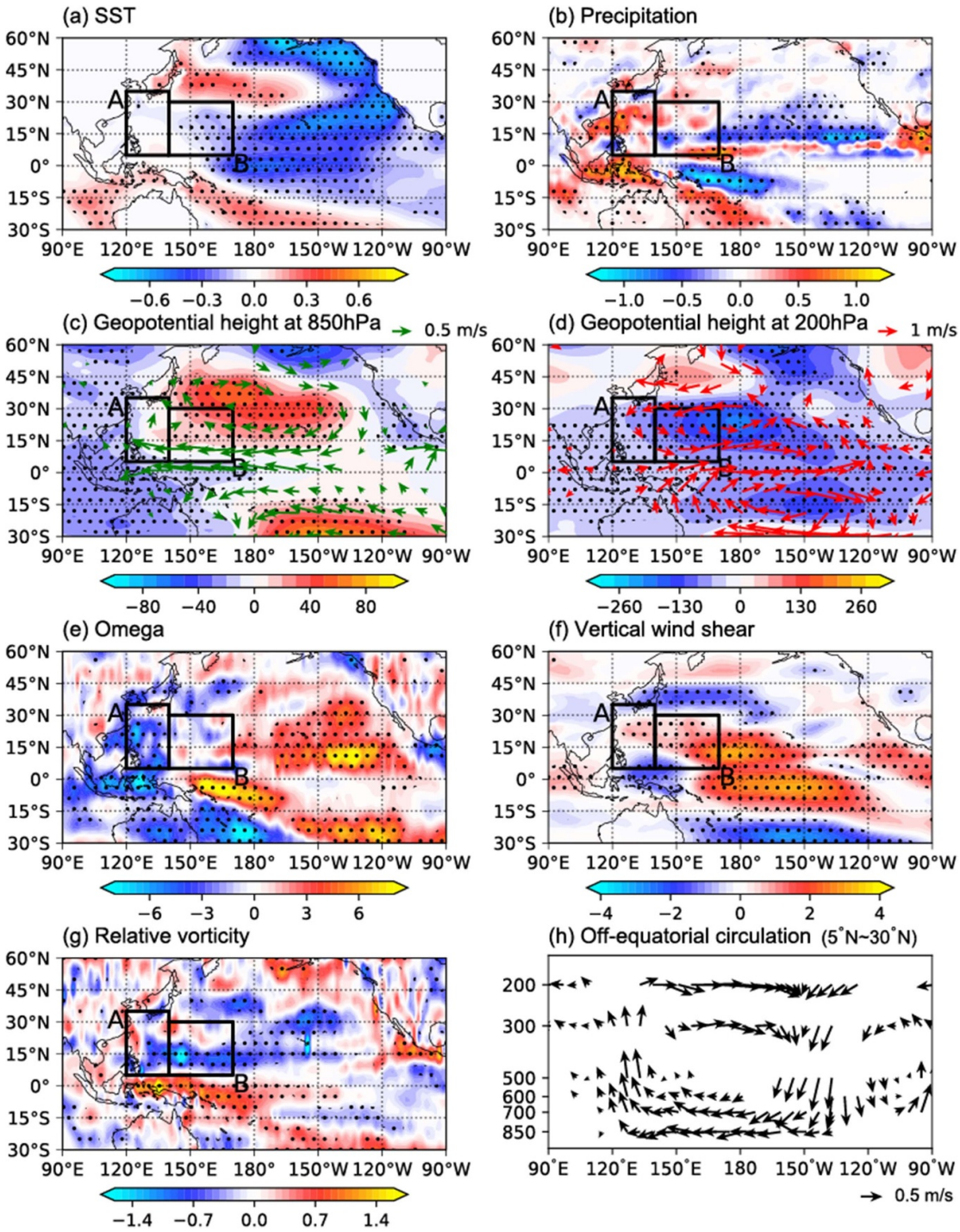

Figure 4. The PC1-regressed fields of (a) SST (°C), (b) precipitation (mm d^{-1}), geopotential height (shading, m^2 s^{-2}) and wind field (vector, m s^{-1}) at (c) 850 hPa and (d) 200 hPa, (e) 500 hPa omega (10^{-3} Pa s^{-1}), (f) 850–200 hPa vertical wind shear (m s^{-1}), (g) 600 hPa relative humidity (%) and (h) off-equatorial east–west secondary circulation on a decadal time scale. All data, including PC1, SST and circulations are firstly filtered using a 7 year low-pass Butterworth filter before producing the regression fields. The off-equatorial circulation is composed of vertical velocity (Pa s^{-1}) and zonal wind (m s^{-1}) averaged between 5° N and 30° N. The vertical velocity is multiplied by a scale factor calculated as the mean zonal wind speed divided by the mean vertical velocity. Only a statistically significant wind (vector) at the 95% confidence level is shown.

south-easterlies and high-level north-westerlies in the northern region B (figures 4(c) and (d)). The opposite anomalous wind fields between 850 hPa and 200 hPa then strengthen the VWS in region B, suppressing TCG (figure 4(f)). Meanwhile, the low-level anticyclonic circulation also weakens the 850 hPa relative vorticity, inhibiting TCG (figure 4(g)).

4. Discussion and conclusion

The NPGO is one of the essential Pacific decadal modes of SST and SSH. During the last few decades, the contribution of the NPGO to SST variation in the North Pacific has significantly increased, comparable to the PDO. However, the impact of the NPGO on

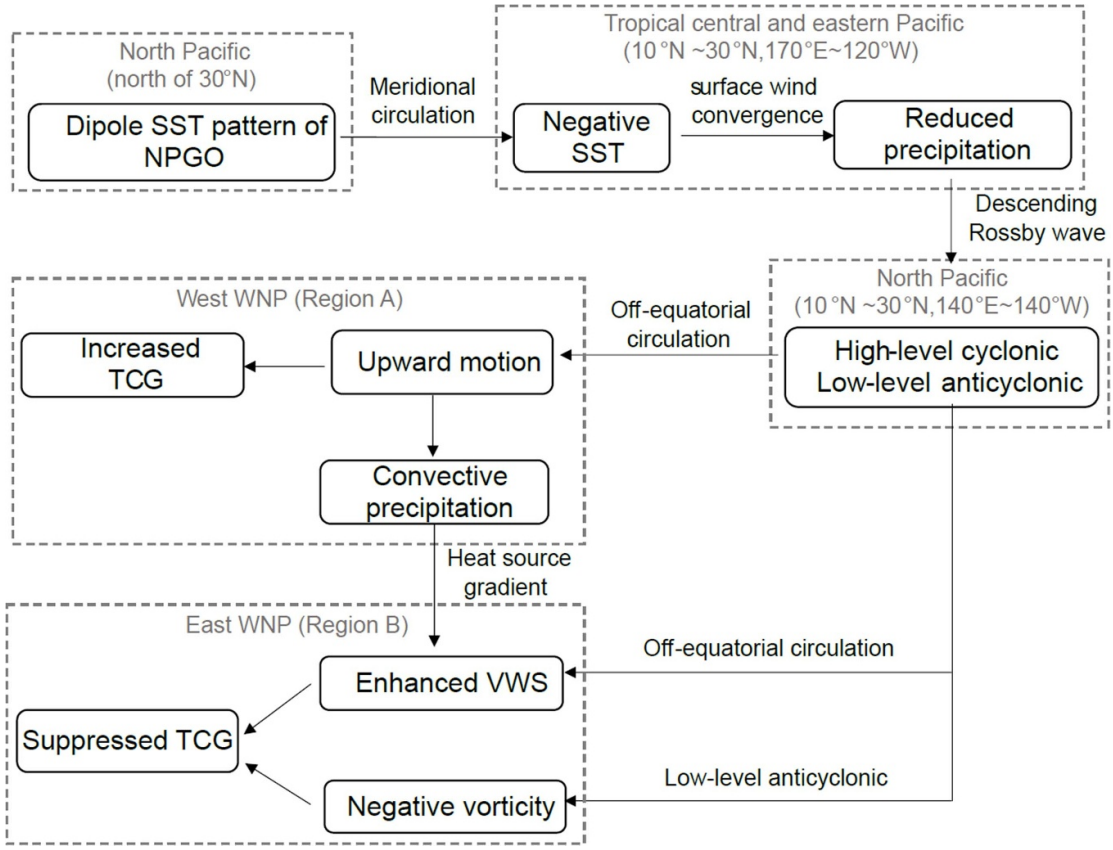

Figure 5. Consequential box diagram of the mechanism by which the NPGO affects WNP TCG.

TC change has rarely been studied. Here we investigated the influence of the NPGO on spatial characteristics of TCG over the WNP on a decadal time scale from 1965 to 2020 and illustrated its underlying mechanisms.

We use EOF analysis to separate the PDO and NPGO modes during the recent 60 years. The NPGO is the first leading EOF mode from JASO North Pacific SST, while the PDO becomes the second EOF mode (figure 1). We detected significant decadal variations (~12 years) from the time series of both PC1 and WNP total TCG during the whole period from 1965 to 2020. The correlation coefficient between PC1 and TCG is −0.49 on a decadal time scale.

The NPGO shows large-scale opposite impacts in west and east of 140° E (figure 3). The negative correlations between PC1 and TCG in the east WNP are statistically significant at most grid points, while the positive correlations in the west WNP are relatively weaker. The asymmetric seesaw correlation pattern results in an overall significant negative correlation in the WNP. The influence of NPGO on TCG is associated with NPGO-induced anomalous large-scale atmospheric and oceanic conditions (figures 2 and 3). The enhanced 500 hPa ascending motion and strengthened VWS are essential factors for NPGO to affect TCG in the west and east of the WNP, respectively.

Figure 5 shows a consequential box diagram illustrating the dynamic control of the TCG by the NPGO-induced SST anomaly and the corresponding circulation anomalies. The EP and TCEP cooling pattern of the NPGO suppresses eastern North Pacific precipitation. The reduced rainfall then results in a descending Rossby wave, leading to North Pacific low-level anticyclonic and upper-level cyclonic anomalies. Thus, the east–west secondary circulation is established with downward motion in the subtropical EP and upward motion in the far WNP. The above anomalous North Pacific circulation enhances the ascent in region A, strengthens VWS in region B and leads to negative low-level vorticity in both regions A and B. The combined effects of VWS, vertical motion and low-level vorticity generate an asymmetric east–west dipole pattern, accounting for suppressed TCG in the east WNP (region B) and slightly increased TCG in the west WNP (region A).

Our findings illuminate the causes of the decadal variations of the TCG in the core regions of the WNP, revealing the critical influence of the NPGO on TCG in the WNP. The results have significant implications for the decadal prediction of change in WNP TCG. Although NPGO-induced large-scale conditions could explain major spatial characteristics of the NPGO–TCG relationship, some remaining issues deserve further exploration. For example, the NPGO

leads to significant favorable and unfavorable conditions in the west and east WNP, respectively, but why is the correlation between NPGO and TCG in most grid points of the west WNP marginally significant? Is the influence of the Atlantic or Indian SST variabilities a possible reason to explain the weak relationship between the NPGO and TCG in the west WNP? Previous studies suggested Atlantic SST variabilities significantly influence WNP TCG on a multidecadal time scale (Zhang *et al* 2018, Wang *et al* 2022). Our 7 year low-pass filter retains the multidecadal variation component that cannot be fully explained by the NPGO mainly on a quasi-decadal time scale. The combined effects of NPGO and Atlantic SST variabilities on WNP TCG are yet to be studied.

Data availability statement

All data used in this study are freely available online. The National Oceanic and Atmospheric Administration Extended Reconstructed SST version 5 (ERSST v5) is derived from: www.ncei.noaa.gov/access/metadata/landing-page/bin/iso?id=gov.noaa.ncdc:C00927. Monthly mean atmospheric circulation and precipitation were obtained from the ERA5 dataset and can be accessed at: https://cds.climate.copernicus.eu/#!/search?text=ERA5&type=dataset. The data that support the findings of this study are available upon reasonable request from the authors.

The data that support the findings of this study are openly available at the following URL/DOI: www.ncei.noaa.gov/products/international-best-track-archive?name=ib-v4-access.

Acknowledgments

This study is jointly supported by the National Natural Science Foundation of China (Grant Nos. 42192554, 42175007, 41905001, 42192552). Yifei Dai also acknowledges support from the Basic Research Fund of CAMs under Grant No. 2022Y016.

ORCID iD

Na Wei https://orcid.org/0000-0002-5541-6068

References

Cai Y, Han X, Zhao H, Klotzbach P J, Wu L, Raga G B and Wang C 2022 Enhanced predictability of rapidly intensifying tropical cyclones over the western North Pacific associated with snow depth changes over the Tibetan Plateau *J. Clim.* **35** 2093–110

Cao X, Liu Y, Wu R, Bi M, Dai Y and Cai Z 2020 Northwestwards shift of tropical cyclone genesis position during autumn over the western North Pacific after the late 1990s *Int. J. Climatol.* **40** 1885–99

Di Lorenzo E *et al* 2008 North Pacific Gyre Oscillation links ocean climate and ecosystem change *Geophys. Res. Lett.* **35** L08607

Di Lorenzo E, Cobb K M, Furtado J C, Schneider N, Anderson B T, Bracco A, Alexander M A and Vimont D J 2010 Central pacific El Nino and decadal climate change in the North Pacific Ocean *Nat. Geosci.* **3** 762–5

Emanuel K A 2005 *Divine Wind* (Oxford: Oxford University Press)

Emanuel K 2018 100 years of progress in tropical cyclone research *Meteorol. Monogr.* **59** 15.1–68

Emanuel K and Nolan D S 2004 Tropical cyclone activity and the global climate system *26th Conf. on Hurricanes and Tropical Meteorolgy*

Gill A E 1980 Some simple solutions for heat-induced tropical circulation *Q. J. R. Meteorol. Soc.* **106** 447–62

Hersbach H *et al* 2020 The ERA5 global reanalysis *Q. J. R. Meteorol. Soc.* **146** 1999–2049

Hong C C, Wu Y K and Li T 2016 Influence of climate regime shift on the interdecadal change in tropical cyclone activity over the Pacific Basin during the middle to late 1990s *Clim. Dyn.* **47** 2587–600

Hoskins B and Wang B 2006 Large-scale atmospheric dynamics *The Asian Monsoon* (Berlin: Springer) pp 357–415

Hu J, Li T and Xu H 2018 Relationship between the North Pacific Gyre Oscillation and the onset of stratospheric final warming in the northern Hemisphere *Clim. Dyn.* **51** 3061–75

Huang B, Thorne P W, Banzon V F, Boyer T, Chepurin G, Lawrimore J H, Menne M J, Smith T M, Vose R S and Zhang H-M 2017 Extended reconstructed sea surface temperature, version 5 (ERSSTv5): upgrades, validations, and intercomparisons *J. Clim.* **30** 8179–205

Knaff J A, Sampson C R and DeMaria M 2005 An operational statistical typhoon intensity prediction scheme for the western North Pacific *Weather Forecasting* **20** 688–99

Knapp K R, Diamond H J, Kossin J P, Kruk M C and Schreck C J 2018 International best track archive for climate stewardship (IBTrACS) project, Version 4 (NOAA National Centers for Environmental Information) (https://doi.org/10.25921/82ty-9e16)

Li R C Y and ZHOU W 2018 Revisiting the intraseasonal, interannual and interdecadal variability of tropical cyclones in the western North Pacific *Atmos. Oceanic Sci. Lett.* **11** 198–208

Li X, Cheng X, Fei J, Huang X and Ding J 2022 The modulation effect of sea surface cooling on the eyewall replacement cycle in Typhoon Trami (2018) *Mon. Weather Rev.* **150** 1417–36

Lindzen R S and Nigam S 1987 On the role of sea surface temperature gradients in forcing low-level winds and convergence in the tropics *J. Atmos. Sci.* **44** 2418–36

Litzow M A, Hunsicker M E, Bond N A, Burke B J, Cunningham C J, Gosselin J L, Norton E L, Ward E J and Zador S G 2020 The changing physical and ecological meanings of North Pacific Ocean climate indices *Proc. Natl Acad. Sci. USA* **117** 7665–71

Liu Y and Chen G 2018 Intensified influence of the ENSO Modoki on boreal summer tropical cyclone genesis over the western North Pacific since the early 1990s *Int. J. Climatol.* **38** e1258–65

Lorenz E N 1956 *Empirical Orthogonal Functions and Statistical Weather prediction[M]* (Cambridge, MA: Massachusetts Institute of Technology)

Lu G Y and Wong D W 2008 An adaptive inverse-distance weighting spatial interpolation technique *Comput. Geosci.* **34** 1044–55

Ma Z and Fei J 2022 A comparison between moist and dry tropical cyclones: the low effectiveness of surface sensible heat flux in storm intensification *J. Atmos. Sci.* **79** 31–49

Mantua N J, Hare S R, Zhang Y, Wallace J M and Francis R C 1997 A Pacific interdecadal climate oscillation with impacts on salmon production *Bull. Am. Meteorol. Soc.* **78** 1069–80

Matsuno T 1966 Quasi-geostrophic motions in the equatorial area *J. Meteorol. Soc. Japan* II **44** 25–43

North G R, Bell T L, Cahalan R F and Moeng F J 1982 Sampling errors in the estimation of empirical orthogonal functions *Mon. Weather Rev.* **110** 699–706

Patricola C M, Camargo S J, Klotzbach P J, Saravanan R and Chang P 2018 The influence of ENSO flavors on

western North Pacific tropical cyclone activity *J. Clim.* **31** 5395–416
Pu X, Chen Q, Zhong Q, Ding R and Liu T 2019 Influence of the North Pacific Victoria mode on western North Pacific tropical cyclone genesis *Clim. Dyn.* **52** 245–56
Ren F, Wu G, Dong W, Wang X, Wang Y, Ai W and Li W 2006 Changes in tropical cyclone precipitation over China *Geophys. Res. Lett.* **33** L20702
Rogers J C 1981 The north Pacific oscillation *J. Climatol.* **1** 39–57
Song J, Klotzbach P J and Duan Y 2021 Recent weakening of the interannual relationship between ENSO Modoki and boreal summer tropical cyclone frequency over the western North Pacific *J. Meteorol. Soc. Japan* II **99** 1071–88
Wang B and Chan J C L 2002 How strong ENSO events affect tropical storm activity over the western North Pacific *J. Clim.* **15** 1643–58
Wang B, Luo X, Yang Y-M, Sun W, Cane M A, Cai W, Yeh S-W and Liu J 2019 Historical change of El Niño properties sheds light on future changes of extreme El Niño *Proc. Natl Acad. Sci.* **116** 22512–7
Wang B and Murakami H 2020 Dynamic genesis potential index for diagnosing present-day and future global tropical cyclone genesis *Environ. Res. Lett.* **15** 114008
Wang B, Yang Y, Ding Q-H, Murakami H and Huang F 2010 Climate control of the global tropical storm days (1965–2008) *Geophys. Res. Lett.* **37** L07704
Wang C, Wang B, Wu L and Luo J-J 2022 A seesaw variability in tropical cyclone genesis between the Western North Pacific and the North Atlantic shaped by Atlantic multidecadal variability *J. Clim.* **35** 2479–89
Wang L, Huang R and Wu R 2013 Interdecadal variability in tropical cyclone frequency over the South China Sea and its association with the Indian Ocean Sea surface temperature *Geophys. Res. Lett.* **40** 768–71
Wu B, Lin X and Yu L 2020 North pacific subtropical mode water is controlled by the Atlantic multidecadal variability *Nat. Clim. Change* **10** 238–43
Xiao D and Li J P 2007 Spatial and temporal characteristics of the decadal abrupt changes of global atmosphere-ocean system in the 1970s *J. Geophys. Res.* **112** D24S22
Ye X, Zhang W and Luo M 2016 The North Pacific gyre oscillation and East Asian summer precipitation *Atmos. Sci. Lett.* **17** 531–7
Zhang Q, Wu L and Liu Q 2009 Tropical cyclone damages in China 1983–2006 *Bull. Am. Meteorol. Soc.* **90** 489–96
Zhang W, Leung Y and Min J 2013 North Pacific Gyre Oscillation and the occurrence of western North Pacific tropical cyclones *Geophys. Res. Lett.* **40** 5205–11
Zhang W, Vecchi G A, Murakami H, Villarini G, Delworth T L, Yang X and Jia L 2018 Dominant role of Atlantic multidecadal oscillation in the recent decadal changes in western North Pacific tropical cyclone activity *Geophys. Res. Lett.* **45** 354–62
Zhao H and Wang C 2019 On the relationship between ENSO and tropical cyclones in the western North Pacific during the boreal summer *Clim. Dyn.* **52** 275–88
Zhao H, Zhao K, Klotzbach P J, Wu L and Wang C 2022 Interannual and interdecadal drivers of meridional migration of Western North Pacific tropical cyclone lifetime maximum intensity location *J. Clim.* **35** 2709–22